This article has been accepted for publication in a future issue of this journal, but has not been fully edited. Content may change prior to final publication. Citation information: DOI 10.1109/TPWRS.2016.2598548, IEEE Transactions on Power Systems

Corrective Model-Predictive Control in Large Electric Power Systems

Jonathon A. Martin, *Student Member, IEEE* Ian A. Hiskens, *Fellow, IEEE*

***Abstract*—Enhanced control capabilities are required to coordinate the response of increasingly diverse controllable resources, including FACTS devices, energy storage, demand response and fast-acting generation. Model-predictive control (MPC) has shown great promise for accommodating these devices in a corrective control framework that exploits the thermal overload capability of transmission lines and limits detrimental effects of contingencies. This work expands upon earlier implementations by incorporating voltage magnitudes and reactive power into the system model utilized by MPC. These improvements provide a more accurate prediction of system behavior and enable more effective control decisions. Performance of this enhanced MPC strategy is demonstrated using a model of the Californian power system containing 4259 buses. Sparsity in modelling and control actions must be exploited for implementation on large networks. A method is developed for identifying the set of controls that is most effective for a given contingency. The proposed MPC corrective control algorithm fits naturally within energy management systems where it can provide feedback control or act as a guide for system operators by identifying beneficial control actions across a wide range of devices.**

***Index Terms*—Power system control; Power system modeling; Model predictive control; Corrective control; Power system operation; Dynamic line rating.**

I. Introduction

RELIABLE operation of electric power systems depends upon system operators continually monitoring system behavior and enacting control decisions. As new technologies emerge and greater investment is directed toward distributed renewable energy assets, traditional operating strategies must adapt accordingly. Faced with a large number of small distributed devices, system operators will find it more challenging to quickly identify the most useful control actions during system events. Methods which are capable of operating in real-time to provide feedback control or decision support will provide a valuable resource to system operators as they respond to stressed network conditions.

The development of tools to identify corrective actions has been of interest for several decades. These algorithms must be capable of considering a variety of control devices while operating quickly and reliably [1], and have traditionally been divided between power redispatch [2]–[5] and transmission switching [6]–[8]. The binary nature of switching actions requires mixed-integer models which are difficult to solve in real-time for large networks. In contrast, linear models offer straightforward implementation for large-scale systems but must be carefully tailored to cater for power system nonlinearities [9], [10].

Model-predictive control (MPC) provides a systematic approach to resolving discrepancies arising from the use of linear models for controlling nonlinear systems [11], [12]. MPC uses an internal (approximate) model of the system to predict behavior and establish an optimal control sequence. The control actions from the first step of this sequence are implemented on the actual system. Subsequent measurement of the resulting system behavior provides the initial conditions for MPC to again predict behavior and recalculate an optimal control sequence. The feedback inherent in the repetition of this process allows MPC to control a broad range of devices while effectively satisfying a multi-period constrained optimal power flow problem.

Early investigations into the use of MPC for relieving thermal overloading of transmission lines were undertaken in [13], [14]. To return line currents to within their long-term ratings following a contingency, MPC regulated the angle on phase-shifting transformers, redispatched generation, and shed load as a last resort. The study found that both the length of the prediction horizon and the accuracy of the network model can have an appreciable influence on the ability of MPC to meet its control objectives.

The work presented in [15] further expanded on these ideas by incorporating a temperature-based model of transmission lines [16], [17]. Enforcing a temperature limit on a transmission line while considering actual ambient conditions provides greater flexibility than the conservative assumptions typically used in device ratings. Employing a temperature model of transmission lines has been possible for several decades using dynamic line rating technologies [18]–[21]. The authors of [15] pointed out that moving to a temperature-based model of transmission line loading reduces the likelihood of incorrect operation of the control scheme.

The shift toward distributed renewable generation and energy storage technologies has motivated further investigation of MPC-based cascade mitigation. In [22], [23], brief temperature overloads are relieved using energy storage and curtailment of renewables in addition to the control measures utilized in [13], [15]. This work demonstrated the ability of MPC to prevent cascading overloads in small test networks. To do so, it made use of a linear dc power flow formulation. In contrast, real power systems have thousands of buses and branches, and voltage and reactive power considerations become increasingly important during major contingencies. This current paper therefore expands upon the MPC methodology presented in [22], [23] to account for voltage magnitudes and reactive power. The improved model identifies more

This work was supported by ARPA-E under research grant DE-AR0000232 and by the National Science Foundation through grant CNS-1238962.

The authors are with the Department of Electrical Engineering and Computer Science, University of Michigan, Ann Arbor, MI 48109 USA (e-mail: jandrewm@umich.edu; hiskens@umich.edu).

This article has been accepted for publication in a future issue of this journal, but has not been fully edited. Content may change prior to final publication. Citation information: DOI 10.1109/TPWRS.2016.2598548, IEEE Transactions on Power Systems

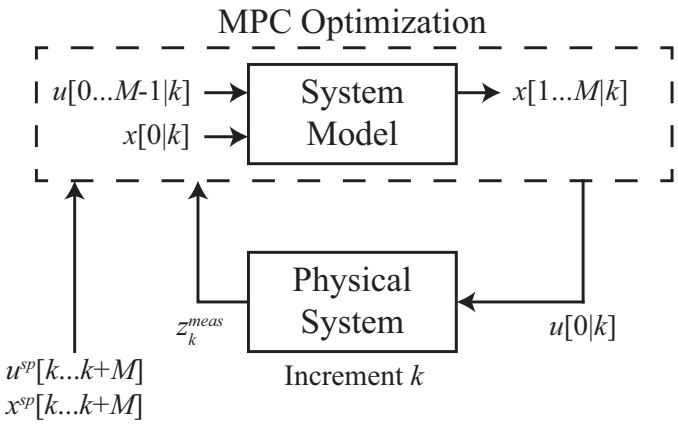

Fig. 1. Overview of MPC strategy.

appropriate control actions which limit detrimental thermal behavior. Additionally, an approach to extending control to large networks is developed and demonstrated on a 4259-bus model of the Californian electricity network.

The outline of this paper is as follows. Section II describes the controller formulation and updated device models. Section III presents improved power flow and line loss models. A technique to reduce the computational burden of large networks is developed in Section IV, with Section V providing a demonstration using the Californian network. Finally, Section VI concludes the paper.

II. Controller Formulation

A. Model-predictive control

The term MPC does not refer to a specific control strategy but rather to a class of strategies which utilize a process model to establish a control sequence that minimizes an objective function over a specified horizon [11]. If the horizon is finite or the model imperfect, the strategy is repeated as time progresses and new information becomes available. The proposed MPC strategy repeatedly solves a form of multi-period optimal power flow that considers slower dynamic processes associated with transmission line conductor temperature, energy storage state-of-charge, and ramp-limited generation. For such processes, a controller response rate on the order of one to two minutes is sufficient. Sub-second voltage and generator transients are significantly faster than the time constants of these slower processes. It is assumed fast transients are stabilized by standard closed-loop controls, e.g. generator AVRs/PSSs, and are ignored in the MPC model.

Fig. 1 outlines the MPC control strategy. At time k, all measurements necessary to model the network, z_k^{meas}, are provided to the controller. These measurements include voltages, generation, storage state-of-charge, device operating states, network configuration, transmission line temperatures, and the most recent load and renewable forecasts. This information is obtained from SCADA/PMU measurements and state estimation[1], and determines the initial value of the system state, $x[0|k]$. MPC then builds an optimization problem to determine a control sequence, $u[0 \dots M-1|k]$, over a horizon of M time-steps while considering its effects on states, $x[1 \dots M|k]$, using a model of the network. The controls are selected to track scheduled set-point values[2] for both the controls, $u^{sp}[k \dots k+M-1]$, and states, $x^{sp}[k+1 \dots k+M]$, over the prediction horizon. Once an optimal control sequence is identified, the controls from the first step in the sequence, $u[0|k]$, are applied to the physical system. The physical system responds to the controls as time advances from k to $k+1$, and the process repeats when new system measurements, z_{k+1}^{meas}, become available.

The MPC strategy extends naturally to power system applications due to its compatibility with present economic dispatch techniques. The MPC formulation presented in this work operates every minute whereas traditional security constrained economic dispatch programs operate every five minutes [24], [25]. In the PJM and NYISO networks, severe overloads exceeding the load dump or short-term emergency ratings, respectively, must be resolved within five minutes [25], [26] to prevent tripping of a transmission line which can further exacerbate the problem. MPC identifies an optimal response within this time-frame while considering future effects of the control actions and minimizing deviations from the economic dispatch. In this way, the proposed controller assumes the role of a system operator responding to thermal rating and voltage magnitude concerns in real time while seeking to maintain, as best possible, the economic schedule.

B. Optimization problem

The optimal control problem solved within MPC is a quadratic program (QP). A high level summary of the network model embedded in the program is provided in (1).

$$\begin{array}{ll} \text{minimize} & \text{Deviation from economic dispatch} \\ s.t. & \text{Generator constraints} \\ & \text{Renewable constraints} \\ & \text{Load constraints} \\ & \text{Storage constraints} \\ & \text{Power flow constraints} \\ & \text{Thermal constraints.} \end{array} \tag{1}$$

As a QP, the objective function is quadratic while the constraints are linear. The program considers time-coupled behavior to predict the power system response over the interval $[k, k+M]$. The system dynamics are discretized using forward Euler with sample time T_s. The measured system states z_k^{meas} define the initial states of the MPC model, $x[0|k]$. The discrete control actions $u[0|k]$ identified by MPC are implemented on the physical network in a step-wise manner with constant step-width T_s, giving $u(t) := u[0|k]$ for $t \in [kT_s, (k+1)T_s)$. When the value of k is obvious from context, the notation $u[l|k]$ is condensed to $u[l]$.

The implementation of (1) in this work is similar to that of [22], [23] but with the model extended to incorporate

[1]The time delays inherent in SCADA and state estimation can be ignored as they are small relative to the time constants of the dynamic processes considered in this MPC formulation.

[2]These scheduled values are typically established by economic dispatch.

This article has been accepted for publication in a future issue of this journal, but has not been fully edited. Content may change prior to final publication. Citation information: DOI 10.1109/TPWRS.2016.2598548, IEEE Transactions on Power Systems

voltage magnitudes and reactive power. Many adaptations to the network model are slight and are presented in the remainder of this section for completeness. More significant changes are discussed in Section III.

1) Objective and variables: The objective of (1) is to minimize the cost of corrective actions which deviate from a prespecified dispatch while resolving power system limit violations. The objective function has the form,

$$\left\|x[M]-x^{sp}[M]\right\|_{P_M}+\sum_{l=0}^{M-1}\left(\left\|x[l]-x^{sp}[l]\right\|_{P}+\left\|u[l]-u^{sp}[l]\right\|_{R}\right). \quad (2)$$

The notation $\|y\|_P$ represents the quadratic function $y^\top Py$. The weighting matrices P_M, P, and R are positive definite with larger weights applied to P_M than P to provide flexibility throughout the horizon while encouraging the controller to return to the prespecified dispatch by the end of the prediction horizon.

Not all variables included in the constraints of (1) appear in the objective function (2). Many are internal variables necessary to model the behavior of the various network elements. They will be introduced as the constraints of (1) are further clarified. The state variables $x[l]$ that appear in the objective function are:

- $\Delta\hat{T}_{ij}$: Relaxed temperature overload on line ij, [°C]
- p_{Gn}: Active power output of generator n, [pu]
- q_{Gn}: Reactive power output of generator n, [pu]
- E_n: Energy in storage device n, [pu-hr]
- U_n^+, U_n^-: Over (under)-voltage violation at bus n, [%].

The control variables $u[l]$ are:

- Δp_{Gn}: Change in active power of generator n, [pu]
- p_{Rn}^{cur}: Active power curtailment of renewable n, [pu]
- p_{Dn}^{red}: Active power reduction of load n, [pu]
- $p_{Sc,n}$: Charging power of storage device n, [pu]
- $p_{Sd,n}$: Discharging power of storage device n, [pu]
- ψ_{ij}: Phase angle of phase-shifting transformer ij, [rad].

2) Generator constraints: Within (1), generators are modeled as power sources with ramp-rate limits on their active power production. As such, their active power output is governed by a simple discretized dynamic equation in combination with operating limits on the active and reactive power outputs:

$$p_{Gn}[l+1]=p_{Gn}[l]+\Delta p_{Gn}[l], \quad (3a)$$
$$p_{Gn}[0]=p_{Gn}^{meas}, \quad (3b)$$
$$\Delta p_{Gn}^{min}[l]\le\Delta p_{Gn}[l]\le\Delta p_{Gn}^{max}[l], \quad (3c)$$
$$p_{Gn}^{min}[l]\le p_{Gn}[l]\le p_{Gn}^{max}[l], \quad (3d)$$
$$p_{Gn}^{min}[M]\le p_{Gn}[M]\le p_{Gn}^{max}[M], \quad (3e)$$
$$q_{Gn}^{min}[l]\le q_{Gn}[l]\le q_{Gn}^{max}[l], \quad (3f)$$

for $l\in\{0,\dots,M-1\}$.

Equations (3a) and (3c) ensure that generator active power output does not change more quickly than its ramp-rate limits permit, (3b) initializes the generator output to its measured value at the start of the prediction horizon, and (3d)-(3f) maintain the active and reactive power within their respective limits.

3) Renewable constraints: Renewable generators are assumed to operate at unity power factor and only have the ability to curtail their active power output:

$$p_{Rn}^{nom}[l]=p_{Rn}[l]+p_{Rn}^{cur}[l], \quad (4a)$$
$$0\le p_{Rn}^{cur}[l]\le p_{Rn}^{nom}[l], \quad (4b)$$

for $l\in\{0,\dots,M-1\}$.

In (4a), the output of the renewable source, p_{Rn}, plus any curtailment must equal the nominal forecast, p_{Rn}^{nom}. Curtailment remains within limits due to (4b).

4) Load constraints: Loads consume power at a fixed power factor and can be reduced if necessary:

$$p_{Dn}^{nom}[l]=p_{Dn}[l]+p_{Dn}^{red}[l], \quad (5a)$$
$$q_{Dn}^{nom}[l]p_{Dn}[l]=p_{Dn}^{nom}[l]q_{Dn}[l], \quad (5b)$$
$$0\le p_{Dn}^{red}[l]\le p_{Dn}^{nom}[l], \quad (5c)$$

for $l\in\{0,\dots,M-1\}$.

In (5a), the demand of the load, p_{Dn}, plus any reduction must equal the nominal forecast, p_{Dn}^{nom}. Equation (5b) ensures that the reactive power of the load, q_{Dn}, is appropriately adjusted from its nominal forecast, q_{Dn}^{nom}, to maintain a constant power factor when active demand is reduced. Demand reduction limits are enforced by (5c)

5) Storage constraints: Storage devices are limited-energy devices:

$$E_n[l+1]=E_n[l]+T_s\eta_{c,n}p_{Sc,n}[l]-\frac{T_s}{\eta_{d,n}}p_{Sd,n}[l], \quad (6a)$$
$$E_n[0]=E_n^{meas}, \quad (6b)$$
$$p_{Sn}[l]=p_{Sc,n}[l]-p_{Sd,n}[l], \quad (6c)$$
$$0=p_{Sc,n}[l]p_{Sd,n}[l], \quad (6d)$$
$$0\le p_{Sc,n}[l]\le p_{Sc,n}^{rate}, \quad (6e)$$
$$0\le p_{Sd,n}[l]\le p_{Sd,n}^{rate}, \quad (6f)$$
$$0\le E_n[l]\le E_n^{rate}, \quad (6g)$$
$$0\le E_n[M]\le E_n^{rate}, \quad (6h)$$

for $l\in\{0,\dots,M-1\}$.

The relationship between energy, charging, and discharging in a storage device is established by (6a). The charging and discharging efficiencies, $\eta_{c,n}$ and $\eta_{d,n}$ respectively, describe the losses in the energy conversion process. The energy is initialized to its measured value using (6b). The net power demand of storage, p_{Sn}, is given by (6c). The complementarity condition of (6d) eliminates simultaneous charging and discharging. It is relaxed into a linear formulation using the approximation described in Appendix A of [22]. The power and energy capability limits of the device are enforced by (6e)-(6h).

6) Thermal constraints: Transmission line flow limits are modelled according to thermal characteristics rather than power flow, thus permitting brief overloads beyond the normal rating during emergencies. The thermal dynamics are linearized as described in Section III-D of [22], with the linearization point given by the normal line rating. Hence,

This article has been accepted for publication in a future issue of this journal, but has not been fully edited. Content may change prior to final publication. Citation information: DOI 10.1109/TPWRS.2016.2598548, IEEE Transactions on Power Systems

ΔT_{ij} is defined relative to the line temperature induced by rated flow. This results in the model:

$$\Delta T_{ij}[l+1] = \tau_{ij}\Delta T_{ij}[l] + \rho_{ij}\Delta p_{ij}^{loss}[l] + \mu_{ij}\Delta d_{ij}[l], \quad (7a)$$

$$\Delta T_{ij}[0] = \Delta T_{ij}^{meas}, \quad (7b)$$

$$\Delta T_{ij}[l] \leq \Delta \hat{T}_{ij}[l], \quad (7c)$$

$$0 \leq \Delta \hat{T}_{ij}[l], \quad (7d)$$

$$p_{ij}^{loss}[l] \geq F_c(\delta_i[l], \delta_j[l], U_i[l], U_j[l]), \ \forall c \in \mathcal{C}_{ij}, \quad (7e)$$

for $l \in \{0, \ldots, M-1\}$.

Equation (7a) describes the temperature change ΔT_{ij} from the linearization point due to changes in the losses, $\Delta p_{ij}^{loss} = p_{ij}^{loss} - p_{ij}^{loss,lim}$, and weather conditions, $\Delta d_{ij} = \text{col}(\Delta q_{s,ij}, \ \Delta T_{ij}^{amb})$, with (7b) initializing the temperature to the measured value. Equations (7c)-(7d) ensure that the relaxed temperature excursion $\Delta \hat{T}_{ij}$, which is penalized in the objective function, only takes positive values (corresponding to unacceptably high temperatures). A high terminal penalty is assigned to $\Delta \hat{T}_{ij}$ to encourage acceptable temperature by the end of the horizon. The loss model in (7e) differs from that of [22] to incorporate voltage magnitudes and is discussed in Section III-C.

III. Improved Power Flow

Previous MPC formulations employed a dc power flow model to relate active power injections to line flows. That simplified model provides adequate accuracy under normal operating conditions but is less appropriate as the system becomes stressed. Furthermore, ignoring reactive power flows may underestimate line losses and impede MPC's ability to remove thermal overloads on lines with significant reactive power flows. Also, assuming voltage magnitudes remain fixed at 1 pu may mask unacceptable voltage deviations. Moving to a power flow formulation that is based on the Jacobian of the ac power flow equations addresses these issues while satisfying the QP requirement for linear constraints. This linearized ac formulation of MPC will be referred to as LAC-MPC.

A. Linearized ac power flow constraints

Including voltage magnitudes within the controller model enables voltage limits to be enforced and motivates an improved model for losses. As well as improving accuracy, incorporating reactive power into the LAC-MPC formulation provides additional control options by modeling reactive compensation devices and utilizing the power factor control functionality available in certain devices. The updated power flow constraints are given by,

$$0 = P_n[l] - \sum_{j \in \mathcal{N}} \Big(\frac{\partial P_n}{\partial V_j}\Big|_k V_j[l] \Big) - \sum_{ij \in \mathcal{E}} \Big(\frac{\partial P_n}{\partial \psi_{ij}}\Big|_k \psi_{ij}[l] \Big), \quad (8a)$$

$$0 = Q_n[l] - \sum_{j \in \mathcal{N}} \Big(\frac{\partial Q_n}{\partial V_j}\Big|_k V_j[l] \Big) - \sum_{ij \in \mathcal{E}} \Big(\frac{\partial Q_n}{\partial \psi_{ij}}\Big|_k \psi_{ij}[l] \Big), \quad (8b)$$

for $l \in \{0, \ldots, M-1\}$.

The terms $P_n[l]$ and $Q_n[l]$ respectively represent the sums of all active and reactive power injections at bus n during time-step l, with further details provided in (9). A condensed notation, $V_j = [\delta_j, U_j]^\top$, is used for the voltage angle and magnitude at bus j in the set of nodes $\mathcal{N}$. The coefficients $\frac{\partial P}{\partial V}\big|_k$ and $\frac{\partial P}{\partial \psi}\big|_k$ are the sensitivities of the ac active power equations to changes in voltage angle and magnitude and to changes in transformer phase-shift, respectively. These Jacobian elements are available from the state estimator at time k, the start of the prediction horizon. The coefficients $\frac{\partial Q}{\partial V}\big|_k$ and $\frac{\partial Q}{\partial \psi}\big|_k$ describe similar sensitivities for the reactive power equations. The notation $ij \in \mathcal{E}$ denotes branch ij in the set of branches $\mathcal{E}$.

The net power injection at a bus is determined by summing the individual device injections at that bus. Positive values for generators and renewable sources are treated as injections while positive values for loads and storage devices are treated as demands:

$$P_n[l] = \sum_{j \in \Omega_n^G} p_{Gj}[l] + \sum_{j \in \Omega_n^R} p_{Rj}[l] - \sum_{j \in \Omega_n^D} p_{Dj}[l] - \sum_{j \in \Omega_n^S} p_{Sj}[l], \quad (9a)$$

$$Q_n[l] = \sum_{j \in \Omega_n^G} q_{Gj}[l] - \sum_{j \in \Omega_n^D} q_{Dj}[l]. \quad (9b)$$

for $l \in \{0, \ldots, M-1\}$. The terms Ω_n^G, Ω_n^R, Ω_n^D, and Ω_n^S represent the sets of generators, renewables, loads, and storage devices at bus n, respectively.

The objective function includes a small penalty on changes in a generator's reactive power output relative to the output measured at the start of the prediction horizon. This improves the convergence characteristics of the QP by identifying a unique reactive power allocation when multiple sources are located at the same bus.

B. Voltage magnitude limits

Power system operation must ensure that voltage magnitudes remain within specified limits. These voltage limits can be incorporated into the LAC-MPC formulation as soft constraints, where deviations above or below the acceptable range are penalized in the objective function. Two relaxation variables, U_n^+ and U_n^-, are defined for each bus with,

$$U_n^+[l] \geq U_n[l] - U_n^{max}[l], \quad (10a)$$

$$U_n^-[l] \geq U_n^{min}[l] - U_n[l]. \quad (10b)$$

Both U_n^+ and U_n^- are (quadratically) penalized for deviating from zero. For buses with specified voltage schedules such as generator buses, U_n^{max} and U_n^{min} are both fixed to the scheduled voltage magnitude.

C. Loss model

Voltage magnitudes have a small but meaningful influence on the computation of transmission line losses. Including voltage magnitudes in the loss formulation can reduce errors in the line temperature prediction as the controller responds to

This article has been accepted for publication in a future issue of this journal, but has not been fully edited. Content may change prior to final publication. Citation information: DOI 10.1109/TPWRS.2016.2598548, IEEE Transactions on Power Systems

a disturbance. Improving the loss model therefore reduces the potential for the controller to select erroneous control actions which are unduly optimistic or pessimistic in their prediction of temperature. Consequently, resolving these modelling inaccuracies can reduce the time required for corrective action and decrease the cost of control.

A new line loss formulation which captures the effects of both voltage angle and magnitude is incorporated into the thermal constraints in (7e). This new formulation is based on expressing the loss equation in polar voltage coordinates. For line (i, j), losses are given by,

$$p_{ij}^{loss}(U_i, U_j, \delta_{ij}) = g_{ij}[U_i^2 + U_j^2 - 2U_iU_j\cos(\delta_{ij})], \quad (11)$$

where $\delta_{ij} = \delta_i - \delta_j$. The loss model uses a set of voltage cases $\mathbf{v}_c = [U_{i,c}, U_{j,c}, \delta_{ij,c}]^\top$, $c \in \mathcal{C}_{ij}$, where $\mathcal{C}_{ij}$ includes the measured (state estimator) voltage case $\mathbf{v}_c^{meas}$ together with several other cases that are in the vicinity of $\mathbf{v}_c^{meas}$. These additional cases are selected by considering the Hessian of (11).

When voltage magnitudes U_i and U_j are positive and the angle difference across the line $|\delta_{ij}|$ is less than 90 degrees, the Hessian matrix of (11) will have exactly two positive eigenvalues [27]. When the Hessian is evaluated at the measured voltage case $\mathbf{v}_c^{meas}$, the eigenvectors associated with the positive eigenvalues span a plane centered at $\mathbf{v}_c^{meas}$ over which (11) exhibits locally convex behavior. The additional voltage cases in $\mathcal{C}_{ij}$ are chosen to lie on this plane, and form a circle centered at $\mathbf{v}_c^{meas}$.

Linearizing (11) at each voltage case $\mathbf{v}_c,\ c \in \mathcal{C}_{ij}$ provides the loss model for line (i, j):

$$p_{ij}^{loss}[l] \geq \frac{\partial p_{ij}^{loss}}{\partial \mathbf{v}}\Big|_c \big(\mathbf{v}[l] - \mathbf{v}_c\big) + p_{ij}^{loss}(\mathbf{v}_c), \quad \forall c \in \mathcal{C}_{ij} \quad (12)$$

where $p_{ij}^{loss}[l]$ is the power loss predicted for line (i, j) at time-step l, which is dependent upon the predicted voltages $\mathbf{v}[l]$ at time-step l, with $p_{ij}^{loss}(\mathbf{v}_c)$ calculated using (11). This loss model closely describes the true nonlinear loss function (11) while capturing the influence of varying voltage magnitudes. The performance of this model is explored in [27].

The steps required to set up the loss model for a single transmission line are outlined as follows:

1) Find the eigenvalues and eigenvectors of the Hessian matrix of the loss function, $\nabla^2_{\mathbf{vv}} p_{ij}^{loss}(\mathbf{v}_c^{meas})$, for the measured voltage condition.
2) Select additional voltage cases, $\mathbf{v}_c,\ c \in \mathcal{C}_{ij}$, within a relatively small circle on the plane spanned by the eigenvectors associated with the two positive eigenvalues of the Hessian matrix.
3) Define the linear inequality,

$$p_{ij}^{loss} \geq p_{ij}^{loss}(\mathbf{v}_c) + \nabla_{\mathbf{v}} p_{ij}^{loss}(\mathbf{v}_c)^\top(\mathbf{v} - \mathbf{v}_c), \quad (13)$$

for the loss equation at each point $\mathbf{v}_c,\ c \in \mathcal{C}_{ij}$. This set of inequalities defines the loss model in (7e).

This process can be tuned to improve performance when specific voltage changes are likely or more significant. For instance, in networks where voltage magnitudes change little, linearization neighbors can be biased in the direction of the eigenvector which emphasizes changes in angle difference. Further details are provided in [27].

IV. Application to Large Networks

Testing of MPC in [23] highlighted its capabilities and benefits, albeit on the relatively small IEEE RTS-96 network. Practical implementation requires scaling up to realistically sized networks with thousands of elements. Incorporating all those elements into a multiperiod optimization results in high-dimensional problems that incur unacceptably long solution times and can be numerically unstable. This can be addressed, however, by selectively limiting the number of constraints and variables in the problem formulation.

Section IV-A presents a heuristic algorithm for selecting a set of controllable resources that may be called upon by MPC. The algorithm uses line flow sensitivities known as injection shift factors (ISFs) [9]. ISFs describe (to a linear approximation) the change in the flow on a line resulting from a change in the injection at a node[3]. For the active power flow f_{ij} on a line from bus i to bus j, the row vector of ISFs is given by,

$$s_{ij} = \frac{\partial f_{ij}}{\partial[\delta, U]}\Big(\frac{\partial[P, Q]}{\partial[\delta, U]}\Big)^{-1}, \quad (14)$$

where $\frac{\partial f_{ij}}{\partial[\delta,U]}$ is the row vector of partial derivatives of the flow on line (i, j) with respect to the network voltages, and $\frac{\partial[P,Q]}{\partial[\delta,U]}$ is the power flow Jacobian. The only nonzero entries in $\frac{\partial f_{ij}}{\partial[\delta,U]}$ correspond to the end nodes i and j, so sparse matrix methods can be used to form s_{ij} very efficiently.

A. Specifying control devices

The proposed LAC-MPC program is a QP formulation which minimizes control deviations from scheduled values while seeking to reduce line-flow overloads and maintain power balance across the network. To gain an intuitive understanding of the solution to this problem, consider a simple QP which captures the main characteristics of the formulation:

$$\min_x \ (x - x^{sp})^\top Q(x - x^{sp}) \quad (15a)$$

$$\text{s.t.}$$

$$0 = sx - b \quad (15b)$$

$$0 = \mathbf{1}^\top x \quad (15c)$$

where x is the vector of power injections, x^{sp} is the vector of scheduled injections, $Q \succ 0$ is a positive definite weighting matrix, s is the row vector of ISFs for a given line, b is related to the desired power flow on that line and $\mathbf{1}$ is the vector of ones. The program described by (15) seeks to minimize changes from scheduled injections (15a), while achieving a certain line flow (15b) and maintaining power balance (15c). The Lagrangian for this program is,

$$\mathcal{L}(x, u, v) = x^\top Qx - 2x^{sp\top}Qx + x^{sp\top}Qx^{sp} - u(sx - b) - v(\mathbf{1}^\top x), \quad (16)$$

[3]The slack bus injection must make a compensating adjustment to maintain power balance across the network.

This article has been accepted for publication in a future issue of this journal, but has not been fully edited. Content may change prior to final publication. Citation information: DOI 10.1109/TPWRS.2016.2598548, IEEE Transactions on Power Systems

where u and v are scalar Lagrangian multipliers. The KKT conditions ($\nabla\mathcal{L} = 0$) require,

$$x = x_{sp} + \frac{1}{2}Q^{-1}s^\top u + \frac{1}{2}Q^{-1}\mathbf{1}v \tag{17a}$$

$$u = \left(s\frac{Q^{-1}}{2}s^\top\right)^{-1}\left(-s\frac{Q^{-1}}{2}\mathbf{1}v - sx_{sp} + b\right) \tag{17b}$$

$$v = \frac{\mathbf{1}^\top\frac{Q^{-1}}{2}s^\top\left(s\frac{Q^{-1}}{2}s^\top\right)^{-1}\left(sx_{sp} - b\right) - \mathbf{1}^\top x_{sp}}{\mathbf{1}^\top\frac{Q^{-1}}{2}\mathbf{1} - \mathbf{1}^\top\frac{Q^{-1}}{2}s^\top\left(s\frac{Q^{-1}}{2}s^\top\right)^{-1}s\frac{Q^{-1}}{2}\mathbf{1}}. \tag{17c}$$

Although (17) has rather involved expressions for the Lagrangian multipliers u and v, the intuition of the solution vector x is fairly straightforward, particularly if the objective weighting matrix is the identity, $Q = I$. Expression (17a) indicates that the solution will seek to match the scheduled injections x_{sp}, but each injection will deviate in proportion to its influence over the flow on the controlled line $s^\top u/2$, and all injections will be shifted uniformly by an offset $\mathbf{1}v/2$ to ensure power balance.

In meshed networks, typically only a subset of buses have significant influence over the flow on a specific line. Consequently, the ISF vector s will often have a few dominant nonzero entries while the remaining entries are all relatively small. If a bus has a small entry in the ISF vector s for every line under consideration then varying the injection at that location will have negligible effect on all the flows of interest. Such buses can therefore be fixed to their scheduled injection values and removed from the set of controls. This idea of ignoring less effective controls, and thereby reducing the problem size, extends naturally to the MPC formulation.

The process of selecting which resources to include in the set of controls and which to ignore is undertaken prior to operation of MPC. Fig. 2 provides an outline of the selection process. This algorithm runs sequentially for every overloaded line, with the aim of identifying a subset of devices that remove the overload while respecting device injection limits. The final set of controls is the union of those identified for each individual overloaded line. If system conditions change significantly during MPC operation, the process reruns to update the set of controls.

In step 1 of Fig. 2, the minimum and maximum injection limits of each control device are determined. These limits should take into account ramp-rate limits and fluctuations in resources such as renewables and controllable loads.

Step 2 of the process calculates the ISF values for the overloaded line and then sorts the values from least to greatest (most negative to most positive) for each line. The outcome of this process is illustrated in Fig. 3 for a line in the Californian electric grid. If a certain bus k has a negative ISF value for line (i, j), then injecting power at bus k and absorbing it at the slack bus will cause a decrease in the power flowing on the line from bus i to bus j. The reverse is true for positive ISF values.

At step 3, a bus is taken from the sorted list and any control devices at that bus are added to the set of control resources. The list was arranged in step 2 so that ISF values are sorted from most negative to most positive. Since the objective of this process is to identify a reduced set of resources necessary to resolve line flow overloads while maintaining power balance, control actions must be balanced between power injections and withdrawals. To achieve this balance, each subsequent bus is selected from alternating ends of the list. This helps to ensure that the most useful control devices are added to the control set while accounting for power balance.

In step 4, the injection capability of each control device is set to its minimum or maximum based on the sign of its ISF value and whether power flow should increase or decrease from bus i to bus j. The flow condition for overloaded line

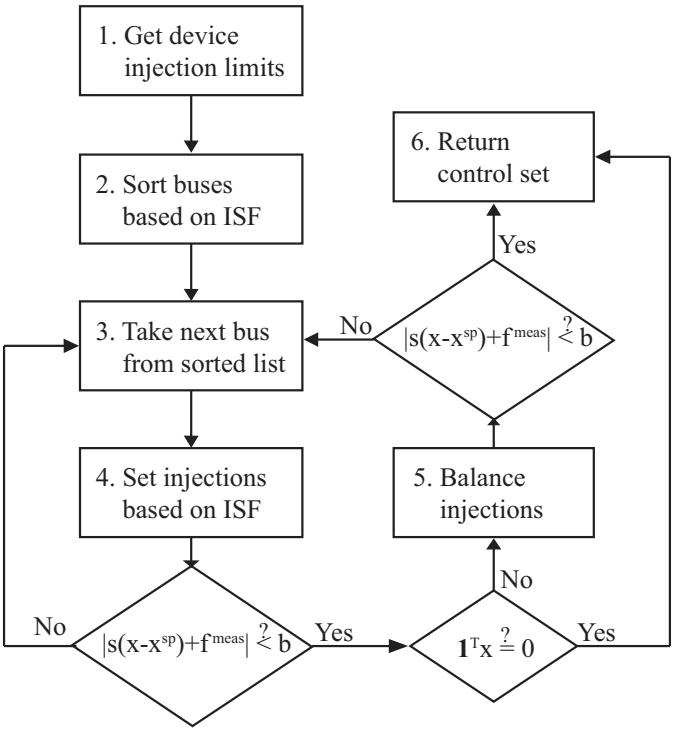

Fig. 2. Process for selecting the set of control devices for each overloaded line.

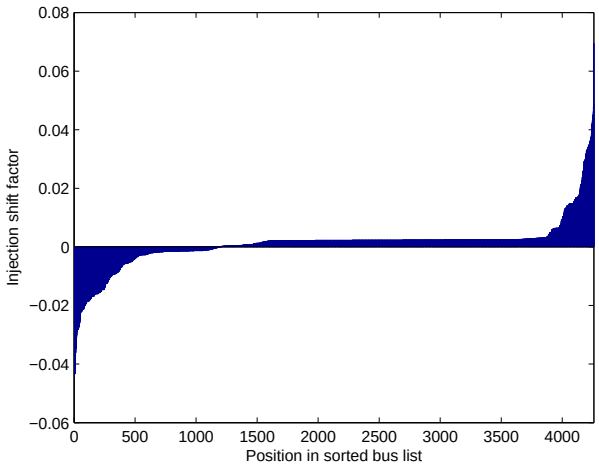

Fig. 3. ISF values ordered from least to greatest, for one particular line in the Californian network.

This article has been accepted for publication in a future issue of this journal, but has not been fully edited. Content may change prior to final publication. Citation information: DOI 10.1109/TPWRS.2016.2598548, IEEE Transactions on Power Systems

(i, j) is then checked to see whether,

$$|s_{ij}(x - x^{sp}) + f_{ij}^{meas}| < b_{ij}, \tag{18}$$

where s_{ij} is the vector of ISF values for line (i, j), x is the vector of device maximum/minimum injections, f_{ij}^{meas} is the actual (overloaded) line flow and b_{ij} is the maximum allowable flow. The entries of x include the control devices which are set to their injection limits and all other devices not in the control set which are held at their scheduled injections x^{sp}. The value of b_{ij} is based on the line rating,

$$b_{ij} = \alpha f_{ij}^{lim}, \tag{19}$$

where α is in the range $(0, 1]$. Smaller values of α will cause the control set to be larger since more control capability will be required to reduce the flow to the tighter limit.

If the flow condition (18) is not satisfied, the process returns to step 3 and adds an additional bus to the control set. If the flow condition is satisfied, the power balance condition is checked. If power balance is achieved within a small tolerance, the process terminates and a sufficient set of control devices has been identified. If power balance has not been achieved, the process moves to step 5, and balances the injections.

In order to balance the power injections at step 5, extra control devices are added to the control set from the appropriate (injection or withdrawal) end of the sorted list until power balance is achieved. The flow condition is then checked once more. If it is satisfied, the process is terminated. If the flow condition is not satisfied, the process returns to step 3 and an additional bus is added to the control set.

By running this process prior to the operation of MPC, a subset of control devices is identified. Only these control devices may be adjusted by MPC and all other devices in the network operate by following their scheduled behavior. This greatly reduces the number of variables in the MPC problem allowing much faster solution. As the control selection process only requires several seconds to operate on a realistically sized network, the cumulative time savings become significant.

B. Specifying thermal models

Additional time-savings can be achieved during solution of the MPC optimization by limiting the number of lines which are represented by thermal models that predict their temperature behavior. Many lines in the network are far from their thermal rating and will remain well below their limit during control actions. If a line does not reach its thermal limit, the corresponding constraints will never be binding and consequently can have no effect on the objective cost or control decisions. Ignoring the thermal dynamics of these lines by not including them in the MPC formulation will not change the outcome but significantly reduces the number of constraints and variables.

At termination of the control set selection process, the predicted injections x^{pred} of every device in the network have been identified. The ISF values for every line in the network are available from (14) and the flow on each line can be predicted, to first order, using,

$$f_{ij}^{pred} = s_{ij}(x^{pred} - x^{sp}) + f_{ij}^{meas}. \tag{20}$$

If the measured or predicted flow on a line is sufficiently close to its rating, it is included in the set of thermally modeled lines. Otherwise, the line does not receive a thermal model in MPC. All lines are still modeled in the network admittance information used in the power flow constraints. As MPC evolves, the predicted flow on each line is monitored. If any lines approach their rating they are added to the set of thermally modeled lines.

C. Power flow reduction

The inclusion of voltage magnitudes and reactive power in the LAC-MPC formulation causes the set of power flow constraints expressed by (8a) and (8b) to become a significant portion of the constraint matrix. Since the power injections of devices outside the set of controls are fixed to their scheduled values, many bus injections are determined prior to MPC operation. Additionally, voltage information is only required to predict losses on thermally modeled lines and to enforce voltage magnitude limits. Since voltage magnitudes tend to be affected locally, voltages remote from the control buses will typically only experience small fluctuations. Buses with noncritical voltages and lacking control capabilities can be eliminated from the power flow constraints using the Kron network reduction technique [28].

The power flow relationship in expressions (8a) and (8b) can be written in matrix form as,

$$\begin{bmatrix} \frac{\partial P}{\partial \delta} & \frac{\partial P}{\partial U} & \frac{\partial P}{\partial \psi} & -I & 0 \\ \frac{\partial Q}{\partial \delta} & \frac{\partial Q}{\partial U} & \frac{\partial Q}{\partial \psi} & 0 & -I \end{bmatrix} \begin{bmatrix} \delta \\ U \\ \psi \\ P \\ Q \end{bmatrix} = \begin{bmatrix} 0 \\ 0 \end{bmatrix}. \tag{21}$$

To apply reduction, the rows and columns of the matrix can be partitioned into two groups. The first group contains all the variables and constraints which are retained in the LAC-MPC model while the second group contains the variables and constraints which are eliminated. The partitioned version of (21) can be expressed as,

$$\begin{bmatrix} A_{11} & A_{12} \\ A_{21} & A_{22} \end{bmatrix} \begin{bmatrix} x_1 \\ x_2 \end{bmatrix} = \begin{bmatrix} d_1 \\ d_2 \end{bmatrix}, \tag{22}$$

where subscript '1' refers to the retained variables and constraints and subscript '2' to those that are eliminated. The variables included in set 2 are terms associated with reduced buses which are 'unknown' in a power flow sense and include voltage angles at PQ and PV buses, voltage magnitudes at PQ buses, and reactive power at PV buses. The constraints included in set 2 are the equations for active and reactive power at reduced buses. Note that the same number of variables and constraints are eliminated, so A_{22} is square.

Applying Kron reduction results in the smaller set of equations, $A_{red}x_1 = d_{red}$, with

$$A_{red} = A_{11} - A_{12}A_{22}^{-1}A_{21}, \tag{23a}$$

$$d_{red} = d_1 - A_{12}A_{22}^{-1}d_2. \tag{23b}$$

Although Kron reduction results in a fairly dense matrix A_{red}, the reduction in problem size typically outweighs the fill-in

This article has been accepted for publication in a future issue of this journal, but has not been fully edited. Content may change prior to final publication. Citation information: DOI 10.1109/TPWRS.2016.2598548, IEEE Transactions on Power Systems

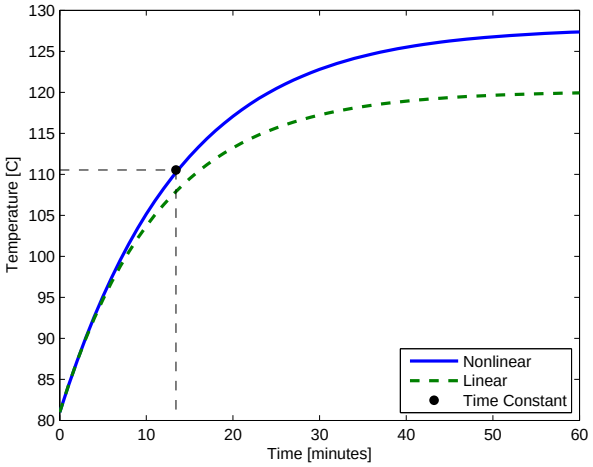

Fig. 4. Temperature response of 26/7 Drake ACSR conductor to a step change in current from 800 A to 1200 A using both nonlinear and linear models. Test conditions are replicated from Figure 2 of [20].

effects. Small terms in A_{red} and d_{red} can be set to zero to reduce fill-in. It is important to note that no accuracy is lost through the reduction process; the only consequence is that eliminated voltage magnitudes can no longer be monitored by MPC.

This power flow reduction coupled with the selection process for control device and line thermal models results in a drastically reduced problem size and vastly improved solution speed. These effects are discussed in the example of Section V-C.

V. Demonstration

A. Thermal model validation

To demonstrate the linearized temperature model (7a), the case-study from Figure 2 in [20] has been reproduced. A 26/7 Drake ACSR conductor undergoes a step change in current from 800 amps to 1200 amps. The actual change in conductor temperature is simulated using the true nonlinear dynamical model with 60 second Euler integration steps. Starting from 81°C, it rises to 128°C, as shown by the solid blue curve in Fig. 4.

The linear model (7a) was subjected to the same step change in current. The coefficients τ_{ij} and ρ_{ij} are determined at the steady-state conditions prior to the step change using the technique presented in Section III-D of [22] and assuming a 60 second time-step. The coefficients in μ_{ij} are not incorporated into the test since ambient conditions do not change, but they could be determined similarly. The thermal behavior predicted by the linear model is shown as the dashed green curve in Fig. 4.

It can be seen from Fig. 4 that both models predict very similar behavior near the linearization conditions. However, the linear model cannot fully describe the variation of resistance and heat transfer with temperature. To minimize the influence of these errors, the dynamics of (7a) are linearized at the current rating of the conductor allowing MPC to accurately predict the thermal behavior of transmission lines near their limit.

Although the concept of a thermal time constant is not directly applicable to the nonlinear model of thermal behavior, it can provide intuition regarding the results. Assuming an exponential curve, the time constant denotes the time required to achieve 63% of the change from the initial temperature to the final value. For the example of Fig. 4, the time constant is 13.4 minutes.

TABLE I
Two-Bus Network Parameters

Parameter	Value	Units
Sampling Time, T_s	60	s
3-phase power base	100	MVA
Line-to-line base voltage	230	kV
Line length	14.5	mi
Line reactance, X_{ij}	0.042	pu
Line shunt susceptance, B_{ij}	0.088	pu
Thermal rating, f_{ij}^{lim}	303	MVA
Ambient Temperature, T_{amb}	35	°C
Wind speed, angle, $v_w \angle \theta_w$	0.61, π/2	m/s, rads
Conductor diameter, D_{ij}	24.2	mm
Heat capacity, $mC_{p,ij}$	958	J/m-°C
Ampacity, I_{ij}^{lim}	760	A
Resistance per unit length	113.5	$\mu\Omega$/m
Temperature limit, T_{ij}^{lim}	86	°C
Temperature coefficient, τ_{ij}	0.886	-
Loss coefficient, ρ_{ij}	0.063	°C-m/W
Solar heat gain rate, $q_{s,ij}$	22.5	W/m

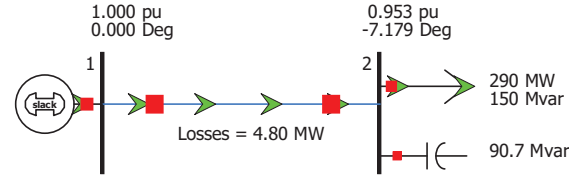

(a)

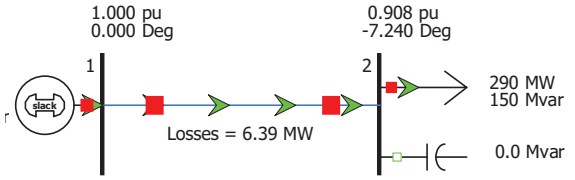

(b)

Fig. 5. Steady-state conditions with a) capacitor connected and b) capacitor disconnected.

B. Comparing dc and linearized ac models

The benefits of using a linearized ac power flow description and the loss model of Section III-C are easily highlighted using a simple two bus power system. A constant load with 100 MVAr capacitive compensation is supplied by a single transmission line strung with 24/7 Peacock ACSR conductor. The network parameters are given in Table I and the steady-state condition is shown in Fig. 5a. The losses are 4.80 MW, and the transmission line temperature settles at 88.2°C.

To disrupt the steady-state conditions, the load bus capacitor is disconnected from the system. The slack generator responds

This article has been accepted for publication in a future issue of this journal, but has not been fully edited. Content may change prior to final publication. Citation information: DOI 10.1109/TPWRS.2016.2598548, IEEE Transactions on Power Systems

to the loss of 90.7 MVAr to balance the network. Both a dc model and a linearized ac model predict the new steady-state voltages and losses. The dc model ignores reactive power and predicts that voltage conditions remain unchanged. The linearized ac formulation of (8a)-(8b) predicts that the load voltage magnitude drops to 0.911 pu and the voltage angle changes to -7.22 degrees.

The voltage predictions of both the dc and linearized ac models are utilized to estimate the new steady-state losses. The dc model uses the piecewise-linear formulation from Section III-B in [22] to describe losses in terms of the squared angle difference. The model discretizes the absolute angle difference across the line into 20 segments of width 0.728 degrees. The linearized ac model predicts losses using the formulation from Section III-C in this work. The (eight) additional voltage cases required for this formulation lie on a circle with radius 0.02 pu around the pre-contingency voltage case.

Although the dc model predicts that voltages remain unchanged, it estimates the new losses to be 4.39 MW instead of remaining at 4.80 MW. This underestimation results from ignoring the off-nominal voltage and reactive power flow which increase losses. The linearized ac model predicts that the new losses are 6.22 MW. The actual change in voltage and losses is found using a power flow and the results are presented in Fig. 5b.

The actual temperature change of the transmission line is determined using the power flow losses and the nonlinear thermal dynamics. The response is shown by the solid black curve of Fig. 6, where the capacitor is disconnected at minute five. The losses given by the dc and linearized ac (LAC) models are used to predict the thermal response, with the results given by the dashed curves of Fig. 6. The linearized ac estimation of losses is much closer to the actual losses than the dc estimation and provides a good approximation[4] of the thermal response. The dc method actually predicts a drop in temperature rather than a rise as it ignores reactive power and underestimates the losses.

This simple example highlights the importance of incorporating reactive power and voltage magnitudes into the MPC formulation. A dc implementation could predict that a transmission line is secure, even though emergency intervention is actually required. Such erroneous operation could later necessitate more extreme control action or lead to equipment damage or unnecessary tripping if the conductors reached a sufficiently high temperature. A linearized ac formulation avoids this situation by anticipating the temperature rise and directing the controller to take corrective actions immediately following the contingency.

C. Large network demonstration

1) Case-study description: To demonstrate the performance of the LAC-MPC formulation on a realistically sized network, a model of the California (CA) transmission grid was obtained together with hourly generation and load data. The model has

[4]The error in the linearized ac prediction of losses will be corrected through the feedback inherent in the MPC process.

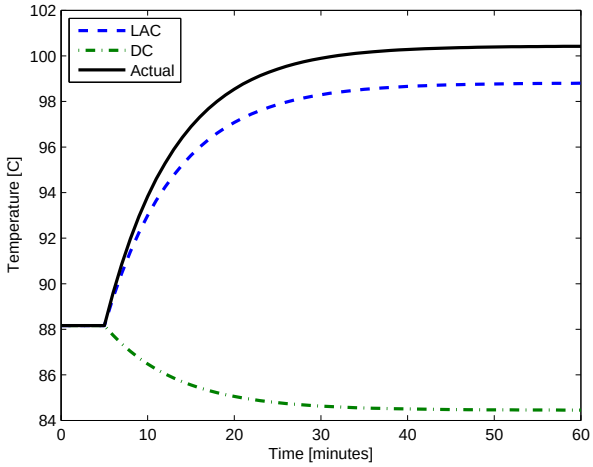

Fig. 6. Temperature response of the transmission line in Fig. 5 due to capacitor disconnection at minute five. The predictions of linear models based on dc and linearized ac (LAC) techniques are compared to the actual response.

4259 nodes, 5867 lines/transformers, 2029 traditional and renewable generators and 1443 loads. Ten energy storage devices were added to the network using the approach described in [29]. To respect the limited use of storage in realistic networks, the cumulative power capacity of the storage devices was 0.5% of the generation capacity.

Modeling temperature behavior on transmission lines requires the use of detailed information regarding line length and conductor type. This information was not available for the CA network and was estimated based on the resistance, power rating and voltage base of each line.

A line trip during the morning ramp period causes an overload and initiates MPC operation. The overloaded line uses 30/7 Lark ACSR conductor with power flow at 138% of its normal rating immediately following the contingency. Without control intervention, the line temperature rises from 2°C below its rated value to 12°C above its rated value in four minutes and trips out of service.

During the first five minutes of operation, MPC seeks to limit thermal overloads while nominally following the pre-contingency schedule defined by the ac economic dispatch algorithm of [30]. After five minutes, a secure post-contingency dispatch becomes available and the new schedule is provided to MPC as its reference. MPC uses a prediction horizon of $M = 10$ steps and a time-step duration of $T_s = 1$ minute. As a comparison, the "human operator" equivalent controller from Section IV-B of [23] is also employed to approximate operator response. This controller penalizes power flow rating violations but does not predict temperature behavior.

The objective coefficients for the MPC and approximate human controllers are given in Table II. The high penalty applied to load reduction indicates that the controller should only utilize demand response if it is absolutely necessary. Additionally, the approximate human controller tends to ignore storage.

As mentioned in Section IV, solving the QP defined by LAC-MPC can be computationally challenging for large net-

This article has been accepted for publication in a future issue of this journal, but has not been fully edited. Content may change prior to final publication. Citation information: DOI 10.1109/TPWRS.2016.2598548, IEEE Transactions on Power Systems

TABLE II
OBJECTIVE FUNCTION COEFFICIENTS

Term	MPC	Human
$\Delta\hat{T}_{ij}$	1	–
p_{Gn}	100	0.01
q_{Gn}	0.1	–
E_n	100	0.01
U_n^+, U_n^-	1000	–
Δp_{Gn}	0.05	0.05
p_{Rn}^{cur}	0.15	0.5
p_{Dn}^{red}	10,000	20,000
$p_{Sc,n}$, $p_{Sd,n}$	0.2	1000
ψ_{ij}	0.01	0.1
Rating violation	–	100

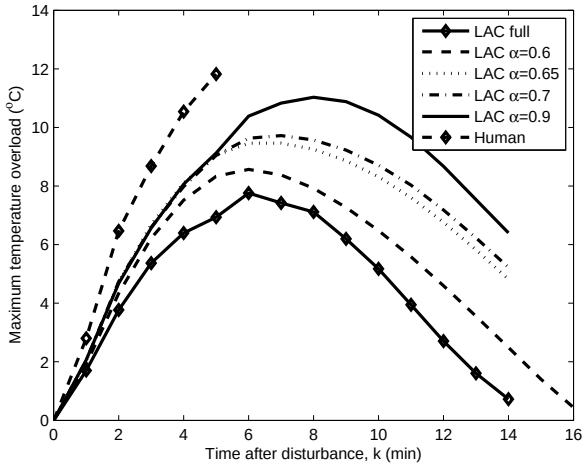

Fig. 7. Maximum temperature overload $\hat{T}_{ij}$ response in the CA network for various control schemes.

works. In this case study, multiple implementations of MPC were compared using different levels of control-set reduction. The algorithm developed in Section IV-A was employed with various values of α in (19) to explore how reducing the retained set of controls affected the ability of LAC-MPC to respond to disturbances. For base-line comparison, the full network complete with all controllable devices was also considered.

Transmission lines with measured or predicted power flows within 70% of their rating were assigned thermal models within MPC. This resulted in 20 transmission lines having thermal models in all MPC implementations.

2) Thermal response: Separate tests were undertaken for six different control implementations: base-line (full network), the reduced control set with $\alpha \in \{0.6, 0.65, 0.7, 0.9\}$, and the approximate human operator. In accordance with the interactions outlined in Fig. 1, the controller guides the network response for at least 14 minutes and terminates once all physical line flows are within 2% of their rating. The maximum temperature of any overloaded line during this process is shown in Fig. 7. No lines outside the thermally modeled set exceeded their power rating at any time.

Each of the LAC-MPC controllers successfully directs the network through the contingency and toward the updated economic dispatch once it becomes available after five minutes

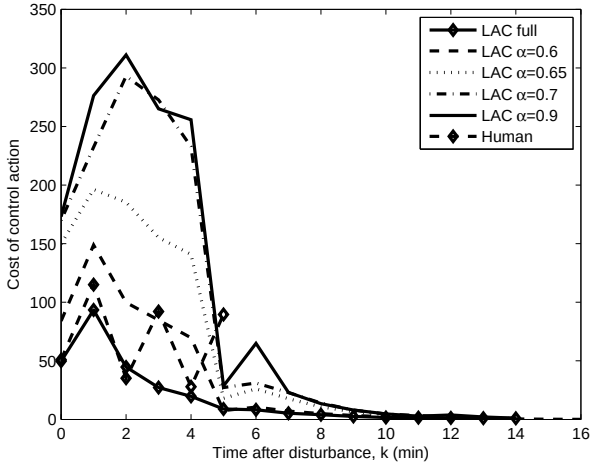

Fig. 8. Cost of implemented controls $u[0|k]$ at each time-step for various control schemes.

of operation. The approximate human controller is unable to suppress the initial temperature rise prior to the updated dispatch, and the overloaded line trips due to unacceptable heating.

In this example, a small amount of load reduction is necessary in addition to the other control options. Although it is expensive, MPC employs a small amount of demand response to satisfy the requirement that thermal overloads be minimized by the end of the prediction horizon. This small adjustment effectively limits the rapid initial temperature increase. The approximate human controller has no terminal requirement on overloads and does not recognize this need for demand response.

The LAC-MPC formulation with control across the full network attains the best temperature profile in Fig. 7. The reduced formulations with $\alpha \in \{0.6, 0.65, 0.7, 0.9\}$ remain close to this trajectory and attain very similar performance to each other during the first five minutes. The variation in temperature at minute six is a result of MPC's balancing actions as network devices outside of the available control set rapidly move toward their new economic set-points.

Smaller values of α require greater control effort to satisfy (19), resulting in MPC retaining control over a larger number of devices. Hence, as α decreases, the control decisions more closely resemble those of MPC with access to the full network. When α reaches 0.59 in this example, all devices in the network are included in MPC's control set. If α is too large, insufficient control is attained and MPC may have difficulty removing all thermal overloads by the end of the prediction horizon.

3) Control cost: Fig. 8 shows the objective cost of the controls implemented on the physical network at each time-step. Again, smaller values of α allow MPC to more closely match the base-line where the entire network is controlled. Only a relatively small number of devices have meaningful influence on the overloaded line as indicated by the injection shift factors in Fig. 3. Values of α between 0.65 and 0.7 include all devices within the peaks at either end of the sorted

TABLE III
COMPUTATIONAL ASPECTS OF LAC-MPC ON THE CA CASE-STUDY

Version	Num. Bus	Mean Sol. Time (s)
full	4259	314
$\alpha = 0.6$	1569	488
$\alpha = 0.65$	934	324
$\alpha = 0.7$	470	10
$\alpha = 0.9$	379	20

ISF list for the overloaded line in this test. Below this value, the control set grows very rapidly for small changes in α because any additional devices have very limited influence on the line flow.

The control costs in Fig. 8 when α is 0.7 or 0.9 are very similar. For α values in this range, controls obtained by decreasing α are effective but expensive and are not significantly utilized by MPC. Alternatively, decreasing α from 0.7 to 0.65 adds cheap but less effective controls. This allows MPC to decrease its costs by balancing the network with less expensive actions as evidenced in Fig. 8, but does not significantly change the temperature response of the overloaded line in Fig. 7.

4) Voltage monitoring: Another benefit of utilizing a linearized ac formulation of MPC is the ability to manage voltage violations. LAC-MPC permits small voltage limit violations using the soft constraints of (10) if they are necessary for feasibility. Alternatively, unacceptable voltage violations are quickly detected and can be eliminated. This type of response is not possible in a dc formulation.

Bus voltages across the network are monitored each time MPC requires updated information about the state of the system. In this demonstration, low voltages are experienced after the first control action of the LAC-MPC formulations operating on the full network and with $\alpha = 0.6$, and also for the approximate human controller. The voltage drop is larger than predicted by MPC at a peripheral bus and results in a 5% low voltage violation. Both MPC methods detect the violation and correct it in the following time-step. The approximate human controller is based on a dc power flow and does not recognize the violation, allowing it to persist. The LAC-MPC methods with smaller control sets do not experience any low voltage conditions.

Slight high voltage violations are experienced outside the control set of all reduced LAC-MPC formulations after the secure dispatch is introduced. The violations are insignificant at less than 0.7% and the buses are not added to the control set of MPC. If the violations were more severe, the buses could be added to the control set allowing the voltages to be considered in formulating subsequent control actions.

5) Solution speed: For each of the LAC-MPC control implementations, Table III provides the number of retained buses and the average solution time required to solve the QP using Gurobi [31]. It is interesting to note that reducing the size of the QP by limiting the number of buses in the control set does not always result in a time reduction. This behavior is partially due to the fill-in effects of reducing the power flow constraints for the smaller α values. The sparsity of the full network equations is lost as constraints are eliminated. However, when enough constraints and variables are eliminated, the benefits of reducing the problem size outweigh the fill-in effects. For instance, the solution time when α is in the range of 0.7 to 0.9 is sufficiently rapid that computations could fit into the 60 second control window. That is not the case for the full network. The increase in solution time when α increases from 0.7 to 0.9 is a result of feasibility challenges. The control set when $\alpha = 0.9$ is just sufficient to provide feasibility, whereas the larger control set when $\alpha = 0.7$ provides greater flexibility and finds a solution more easily.

For large networks where solution speed is a concern, several options are available. The control set and the resulting problem size can be reduced using the techniques presented in this work without significant loss of control capability. A second option is to increase the time-step duration T_s.

VI. CONCLUSION

Incorporating voltage magnitudes and reactive power into MPC-based corrective control improves the accuracy of the control predictions and is able to limit the severity of conductor temperature rise following a contingency. Additionally, a model reduction process allows MPC to be applied to large networks. This is demonstrated on a 4259-bus model of the Californian electricity grid. Model reduction significantly reduces the solution time of the controller, allowing real-time implementation.

Further work will examine the ability of MPC to handle contingencies which lead to voltage collapse due to transformer tapping and reactive power deficiencies. Additionally, the reserve requirements necessary to operate MPC over a variety of contingencies will be investigated. Ensuring that sufficient reserves are available for MPC to provide reliability could allow power systems to operate under a corrective rather than preventive security paradigm. This would reduce the economic costs inherent in maintaining $N-1$ security.

REFERENCES

[1] N. Balu *et al.*, "On-line power system security analysis," *Proc. IEEE*, vol. 80, no. 2, pp. 262-282, Feb. 1992.
[2] A. P. Meliopoulos and A. G. Bakirtzis, "Corrective control computations for large power systems," *IEEE Trans. Power App. Syst.*, vol. 102, no. 11, pp. 3598-3604, Nov. 1983.
[3] L. Lenoir, I. Kamwa, and L. A. Dessaint, "Overload alleviation with preventive-corrective statis security using fuzzy logic," *IEEE Trans. Power Syst.*, vol. 24, no. 1, pp. 134-145, Feb. 2009.
[4] A. Vergnol *et al.*, "Line overload alleviation through corrective control in presence of wind energy," *Electric Power Systems Research*, vol. 81, no. 7, pp. 1583-1591, Jul. 2011.
[5] F. Capitanescu *et al.*, "State-of-the-art, challenges, and future trends in security constrained optimal power flow," *Electric Power Systems Research*, vol. 81, no. 8, pp. 1731-1741, Aug. 2011.
[6] A. A. Mazi *et al.*, "Corrective control of power system flows by line and bus-bar switching," *IEEE Trans. Power Syst.*, vol. 1, no. 3, pp. 258-264, Aug. 1986.
[7] J. G. Rolim and L. J. B. Machado, "A study of the use of corrective switching in transmission systems," *IEEE Trans. Power Syst.*, vol. 14, no. 1, pp.336-341, Feb. 1999.
[8] W. Shao and V. Vittal, "Corrective switching algorithm for relieving overloads and voltage violations," *IEEE Trans. Power Syst.*, vol. 20, no. 4, pp. 1877-1885, Nov. 2005.
[9] A. J. Wood, B. F. Wollenberg and G. B. Sheblé, *Power Generation, Operation and Control*, Third edition, John Wiley and Sons, Inc., 2014.
[10] W. Shao and V. Vittal, "LP-based OPF for corrective FACTS control to relieve overloads and voltage violations," *IEEE Trans. Power Syst.*, vol. 21, no. 4, pp. 1832-1839, Nov. 2006.

[11] E. F. Camacho and C. Bordons, *Model Predictive Control*, 2nd ed. London, UK: Springer-Verlag, 2007.

[12] J. B. Rawlings, "Tutorial overview of model predictive control", *IEEE Control Systems Magazine*, vol. 20, no. 3, pp.38-52, June 2000.

[13] B. Otomega, A. Marinakis, M. Glavic and T. Van Cutsem, "Emergency alleviation of thermal overloads using model predictive control," *PowerTech*, pp. 201-206, Jul. 2007.

[14] B. Otomega, A. Marinakis, M. Glavic and T. Van Cutsem, "Model predictive control to alleviate thermal overloads", *IEEE Trans. Power Syst.*, vol. 22, no. 3, pp. 1384-1385, Aug. 2007.

[15] J. S. A. Carneiro and L. Ferrarini, "Preventing thermal overloads in transmission circuits via model predictive control," *IEEE Trans. Control Syst. Technol.*, vol. 18, no. 6, pp. 1406-1412, Nov. 2010.

[16] H. Banakar, N. Alguacil and F. D. Galiana, "Electrothermal coordination part I: theory and implementation schemes", *IEEE Trans. Power Syst.*, vol. 20, no. 2, pp. 798-805, May 2005.

[17] N. Alguacil, H. Banakar and F. D. Galiana, "Electrothermal coordination part II: case studies", *IEEE Trans. Power Syst.*, vol. 20, no. 4, pp. 1738-1745, Nov. 2005.

[18] B. S. Howington and G. J. Ramon, "Dynamic thermal line rating summary and status of the state-of-the-art technology," *IEEE Trans. Power Del.*, vol. 2, no. 3, pp. 851-858, Jul. 1987.

[19] D. A. Douglass and A. Edris, "Real-time monitoring and dynamic thermal rating of power transmission circuits," *IEEE Trans. Power Del.*, vol. 11, no. 3, pp. 1407-1418, Jul. 1996.

[20] *IEEE Standard for Calculating the Current-Temperature Relationship of Bare Overhead Conductors*, IEEE Standard 738, 2012.

[21] D. J. Morrow *et al.*, "Experimentally validated partial least squares model for dynamic line rating," *IET Renewable Power Generation*, vol. 8, no. 3, pp. 260-268, Apr. 2014.

[22] M. R. Almassalkhi and I. A. Hiskens, "Model-predicitive cascade mitigation in electric power systems with storage and renewables – part I: theory and implementation," *IEEE Trans. Power Syst.*, vol. 30, no. 1, pp. 67-77, Jan. 2015.

[23] M. R. Almassalkhi and I. A. Hiskens, "Model-predicitive cascade mitigation in electric power systems with storage and renewables – part II: case-study," *IEEE Trans. Power Syst.*, vol. 30, no. 1, pp. 78-87, Jan. 2015.

[24] "Transmission and Dispatching Operations Manual," New York Independent System Operator, Rensselaer, NY, Manual 12, Feb. 2016.

[25] C. Pilong, "Balancing Operations," PJM, Audubon, PA, Manual 12, Apr. 28, 2016.

[26] "Emergency Operations Manual," New York Independent System Operator, Rensselaer, NY, Manual 15, Apr. 2016.

[27] J. A. Martin and I. A. Hiskens, "Generalized line loss relaxation in polar voltage coordinates," *IEEE Trans. Power Syst.*, to be published.

[28] F. Dörfler and F. Bullo, "Kron reduction of graphs with applications to electrical networks," *IEEE Trans. Circuits Syst. I, Reg. Papers*, vol. 60, no. 1, pp. 150-163, Jan. 2013.

[29] H. Pandžić *et al.*, "Near-optimal method for siting and sizing of distributed storage in a transmission network," *IEEE Trans. Power Syst.*, vol. 30, no. 5, pp. 2288-2300, Sep. 2015.

[30] J. K. Felder and I. A. Hiskens, "Optimal power flow with storage," in *Power Systems Computation Conference (PSCC)*, Wroclaw, Poland, 2014.

[31] *Gurobi Optimizer Reference Manual*, Version 6.5, Gurobi Optimization, Inc., 2015.

Jonathon A. Martin (S'13) received the B.S. degree in engineering from Messiah College, Mechanicsburg, PA, USA, in 2012 and is currently pursuing his Ph.D. degree in Electrical Engineering: Systems at the University of Michigan, Ann Arbor, MI, USA. His research interests include power systems analysis and control, optimization, and integration of renewable energy sources.

Ian A. Hiskens (F'06) is the Vennema Professor of Engineering in the Department of Electrical Engineering and Computer Science, University of Michigan, Ann Arbor. He has held prior appointments in the Queensland electricity supply industry, and various universities in Australia and the United States. His research interests lie at the intersection of power system analysis and systems theory, with recent activity focused largely on integration of renewable generation and controllable loads. Dr. Hiskens is actively involved in various IEEE societies, and was VP-Finance of the IEEE Systems Council. He is a Fellow of IEEE, a Fellow of Engineers Australia and a Chartered Professional Engineer in Australia.